SUPPLEMENTARY MATERIAL

Microfluidic device with focusing and spacing control of objects for resistance based sorting of droplets and cells

P. Sajeesh[1], S. Manasi[2], M. Doble[2], A. K. Sen[1,*]

[1]*Department of Mechanical Engineering, Indian Institute of Technology Madras, Chennai-600036, India*
[2]*Department of Biotechnology, Indian Institute of Technology Madras, Chennai-600036, India*

Device description and principle

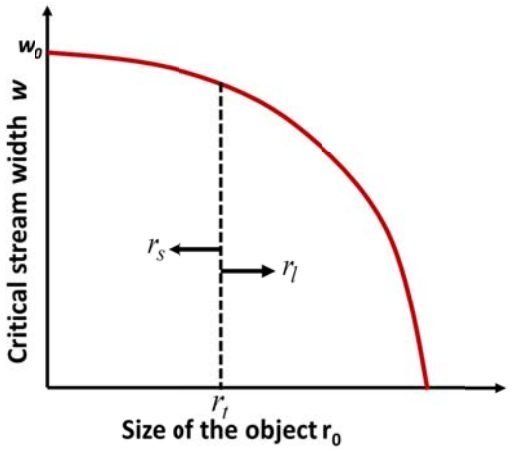

Fig. S1 Schematic of the variation of instantaneous critical stream width w as a function of size of objects r_0

As observed, w is maximum in the absence of any object inside the sensing channel. This initial critical stream width w_0 can be controlled by controlling the flow rate ratio of the side-to-straight channel Q_{si}/Q_{st} (by adjusting the length of the channel segment having resistance R_{si}.

Spacing control

The increase in the spacing between the objects which takes place over a time scale equal to the time taken by the trailing object to get transported by distance g_1 to reach the region *2* is given as $t = g_1/u_{b1}$. The increase in the velocity of the leading object results in an increase in the spacing Δg between the pair of objects which can be expressed as

$$\Delta g = \left(u_{f_2} - u_{f_1}\right)\frac{g_1}{u_{b_1}} \tag{S1}$$

Thus the increased spacing between a pair of objects g_2 in the region *2* is given by

$$g_2 = g_1 + \left(u_{f_2} - u_{f_1}\right)\frac{g_1}{u_{b_1}} \tag{S2}$$

Now, if we consider the mobility of the objects ϕ, which is the ratio of the object velocity u_d to the superficial velocity u_t (i.e. $\phi = u_d/u_t$), the increased spacing can be expressed as

$$g_2 = g_1 + \left(\phi_{f_2}u_{t_2} - \phi_{f_1}u_{t_1}\right)\frac{g_1}{\phi_{b_1}u_{t_1}} \tag{S3}$$

$$g_2 = g_1\left(1+\frac{\phi_{f_2}u_{t_2}}{\phi_{b_1}u_{t_1}}-\frac{\phi_{f_1}}{\phi_{b_1}}\right) \tag{S4}$$

Since the cross-sectional area of the channel in the entire focusing and spacing control region is uniform, the velocities can be replaced with the corresponding flow rates in the region *1* and *2* . Here, u_{t_1} and u_{t_2} are the superficial velocities in region *1* and *2*, respectively.

In earlier work[1] we have found that the mobility of a smaller object is higher as compared to that for a larger object. The spacing predicted using eqn. (S2) is the instantaneous spacing between the objects in region *2* when the trailing object just enters the region *2* and attains a steady velocity u_{b_2} . This new velocity of the trailing object u_{b_2} may be equal, lower or higher as compared to u_{f_2} depending on whether the trailing object is of equal, higher or lower size, respectively as compared to the leading object. Also, for two objects of equal size but different deformability, the mobility of a more deformable object (higher deformability index) is higher as compared to that of a less deformable (lower deformability index) object.[1] Thus, this spacing between the objects will remain fixed if the objects are of equal size (and deformability). However, this spacing will increase or decrease depending on whether the trailing object is larger (or less deformable) or smaller (or more deformable), respectively as compared to the leading object. In a limiting case, when a smaller object follows a larger object in region *2*, thus spacing between the objects continues to decrease. Thus, in order to maintain the required spacing between a pair of objects which is larger than the sensing channel length L_{sen} , the sheath-to-sample flow rate ratio f_{sc} can be appropriately adjusted. An expression of the flow rate ratio f_{sc} required to maintain the required spacing is derived as follows,

$$f_{sc}-\frac{1}{(1+f_{sc})^m}\left[\frac{L_{sen}}{g_1}+\frac{L}{g_1}+\frac{1}{\rho_r^n}-1\right]+\frac{L}{g_1}\frac{1}{(1+f_{sc})^m\rho_r^n}+1=0 \tag{S5}$$

where m and n are the exponents in the relation representing mobility of objects with the capillary number Ca and size ratio ρ of the object, respectively (refer ESI on mobility of objects), g_1 is the initial spacing of objects, ρ_r is the relative size ratio of objects (i.e. the ratio of size of the leading object to the trailing object in a pair) and L is the distance of the region *2* from the sensing channel. The eqn. (S5) can be numerically solved (using MATLAB) to determine the required flow rate ratio to maintain the desired spacing between a pair of adjacent objects.

Focusing control

The analytical solution for the velocity profile in case of flow through a rectangular channel is given by[2],

$$u(y,z)=\frac{4H^2}{\pi^3\mu}\frac{\Delta P}{L}\sum_{n=odd}^{\infty}\frac{1}{n^3}\left[1-\frac{\cosh\left(\frac{n\pi y}{H}\right)}{\cosh\left(\frac{n\pi W_0}{2H}\right)}\right]\sin\left(\frac{n\pi z}{H}\right) \tag{S6}$$

The average velocity across the channel depth $\overline{u(y)}$ $(0\le z\le H)$ can be found out by integrating the velocity profile in the *z*-direction (Ref. Fig. 2) as

$$\overline{u(y)}=\frac{1}{H}\int_0^H u(y,z)\,dz=\frac{8H^2}{\pi^4\mu}\frac{\Delta P}{L}\sum_{n=odd}^{\infty}\frac{1}{n^4}\left[1-\frac{\cosh\left(\frac{n\pi y}{H}\right)}{\cosh\left(\frac{n\pi W_0}{2H}\right)}\right] \tag{S7}$$

The average velocity of the sheath fluid $\bar{u}$ across the channel width in the segments $\left(-\frac{W_0}{2}+D_d\le y\le\frac{W_0}{2}\right)$ of the rectangular channel which is used to focus the sample fluid is written as

$$\bar{u} = \frac{1}{D_d} \int_{-\frac{W_0}{2}+D_d}^{\frac{W_0}{2}} \overline{u(y)}\, dy \tag{S8}$$

Thus, the flow rate of the sheath fluid in region *2* can be derived as follows,

$$q = \frac{H^2}{12\mu}\frac{\Delta P}{L}\left[W_0 - D_d + \sum_{n=odd}^{\infty} \frac{96\,H}{\pi^5 n^5}\left[A - C\left(1+B\right)\right]\right] \tag{S9}$$

where $A = \sinh\left(\frac{n\pi D_d}{H}\right)$, $B = \cosh\left(\frac{n\pi D_d}{H}\right)$, $C = tanh\left(\frac{n\pi W_0}{2H}\right)$ and D_d be the diameter of the smallest object in the sample to be focused by the sheath fluid. Similarly, the average velocity $\overline{U}$ and the flow rate of the sample fluid Q which is focused in the segment $\left(-\frac{W_0}{2} \le y \le -\frac{W_0}{2} + D_d\right)$ of the rectangular channel can be derived out as follows,

$$\overline{U} = \frac{1}{W_0 - D_d} \int_{-\frac{W_0}{2}}^{-\frac{W_0}{2}+D_d} \overline{u(y)}\, dy \tag{S10}$$

$$Q = \frac{H^2}{12\mu}\frac{\Delta P}{L}\left[D_d + \sum_{n=odd}^{\infty} \frac{96\,H}{\pi^5 n^5}\left[C\left(B-1\right) - A\right]\right] \tag{S11}$$

Finally, from eqn. (S9) and (S11), the flow rate ratio $f_p = \frac{q}{Q}$ required for focusing of the objects (of different size) present in a sample is obtained as follows,

$$D_d\left(1+f_p\right) - W_0 + \sum_{n=odd}^{\infty} \frac{96\,H\,f_p}{\pi^5 n^5}\left[C\left(B-1\right) - A\right] - \sum_{n=odd}^{\infty} \frac{96\,H}{\pi^5 n^5}\left[A - C\left(1+B\right)\right] = 0 \tag{S12}$$

Sorting

The resistance across a channel segment is obtained using the pressure drop and flow rate relationship for a rectangular microchannel as[2],

$$R_i = \frac{\Delta p}{Q} = \frac{12\mu L_i}{W_0 H^3\left(1 - \frac{192}{\pi^5}\frac{H}{W_0}\sum_{n=odd}^{\infty}\frac{1}{n^5}\tanh\left(n\pi W_0/2H\right)\right)} \tag{S13}$$

where W_0 and H are the channel width and height, respectively, L_i is the length of the channel segment and μ is the fluid viscosity. The total resistance across the sensing channel varies due to the variable resistance ΔR which depends on the size and deformability of the object that arrives at the sensing channel.[1] For a fixed input current I, the currents in different branches of the network can be found by simplifying the $R_b - R_{sen} - R_{si_1}$ Δ- network into a R_α - R_β - R_γ Y-network through suitable transformations, as shown in Fig. S2. The transformed resistances are obtained as,

$$R_\alpha = \frac{R_{sen}R_b}{R_{sen} + R_b + R_{si}} \tag{S14}$$

$$R_\beta = \frac{R_b\,R_{si}}{R_{sen} + R_b + R_{si}} \tag{S15}$$

$$R_\gamma = \frac{R_{sen}\,R_{si}}{R_{sen} + R_b + R_{si}} \tag{S16}$$

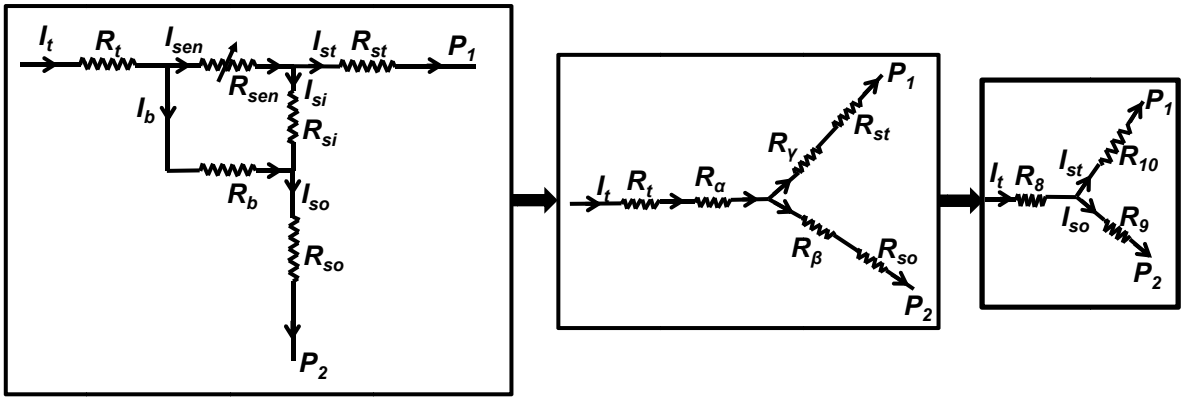

Fig. S2 Equivalent resistance network of the sorting module, showing actual circuit (Δ) and modified circuit (Y)

Applying Kirchhoff's law to the further simplified transformed Y-network, currents in the different branches and hence the flow rates in different channel segments (by converting this electrical circuit back to the hydrodynamic channel network) can be determined as follows,

$$Q_{so} = \frac{Q_t R_{10} - P_2 + P_1}{R_9 + R_{10}} \tag{S17}$$

$$Q_{st} = Q_t - Q_{so} \tag{S18}$$

$$Q_{si} = \frac{P_1 - P_2 + Q_{st} R_{st} - Q_{so} R_{so}}{R_{si}} \tag{S19}$$

$$Q_b = Q_{so} - Q_{si} \tag{S20}$$

$$Q_{sen} = Q_t - Q_b \tag{S21}$$

where $R_8 = R_t + R_\alpha$, $R_9 = R_{so} + R_\beta$ and $R_{10} = R_{st} + R_\gamma$ are the equivalent resistances as shown.

Assuming a three-dimensional fully developed parabolic velocity profile inside the rectangular channel, flow rate in the side branch channel Q_{si} can be derived similar to what is reported for S9 and S11 (ESI on flow focusing) as follows,

$$Q_{si} = \frac{H^2}{12\mu}\frac{\Delta P}{L}\left[w + \sum_{n=odd}^{\infty} \frac{96\,H}{\pi^5 n^5}\left[G(F-1) - E\right]\right] \tag{S22}$$

Similarly, flow rate in the straight branch channel that leads to the outlet *2* can also be derived as follows,

$$Q_{st} = \frac{H^2}{12\mu}\frac{\Delta P}{L}\left[W_0 - w + \sum_{n=odd}^{\infty} \frac{96\,H}{\pi^5 n^5}\left[E - G(1+F)\right]\right] \tag{S23}$$

Size control of objects

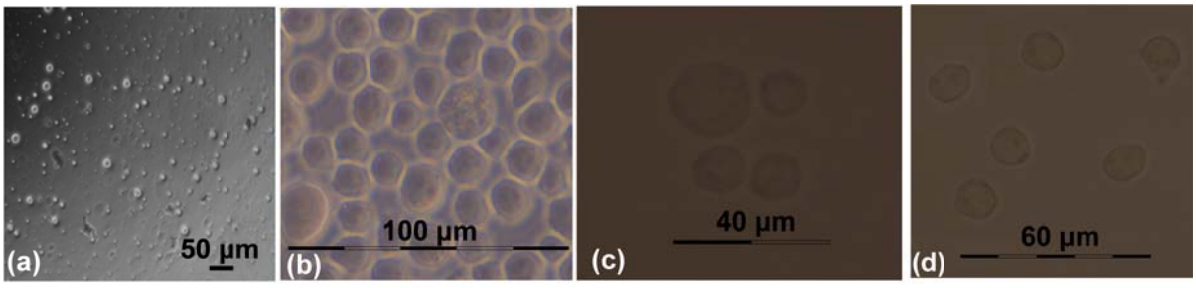

Fig. S3 (a) Emulsions of aqueous glycerol droplets in mineral oil (b) Image showing the cell size variation for <6hrs culture time before dilution (c) after 3-times dilution(d) Images showing uniform size cells for culture time >24hrs.

Mobility of objects

In our earlier work[1], we had reported mobility of droplets (i.e. ratio of droplet velocity to the superficial velocity) in a microchannel for different size and viscosity ratio for Capillary number Ca in the range 0.01–0.2.Since in the present experiments, we are operating at a Capillary number Ca in the range 0.2-1.0 (with a sample flow rate of 0.5µl/min and for a flow rate ratio ranges from 1 to 2), the mobility of the droplets are studied for this range of Ca . The velocity of the droplets was calculated by capturing the movement of the droplets as a function of time using a high speed camera operating at 3000 frames/s. Experiments were performed to measure mobility of droplets at a fixed viscosity ratio ($\lambda = 1.467$) and different size ratio and Capillary numbers, as shown in Fig. S4 (a). Based on the results obtained, the droplet mobility ϕ was correlated with the droplet size ratio ($\rho = 0.3$ -1) and Capillary number Ca as follows,

$$\phi = \frac{A\,Ca^{m}}{\rho^{n}} \tag{S24}$$

where $A = 0.9714$, $m = 0.262$ and $n = 0.1755$ .The correlation was found by curve-fitting a large set of experimental data in MATLAB with R^2 value of 0.85 and 95% confidence bound.

The mobility of cells ϕ_c with the size ratio ρ_c of the cell for a sample flow rate of 2.0 µl/min is shown in Fig. S4 (b). As observed, the mobility of cells decreases with increase in size of the cells which may be due to increased interaction between the cells with the channel wall. For a ~50% increase in cell size, mobility of cells decreases by ~20%.

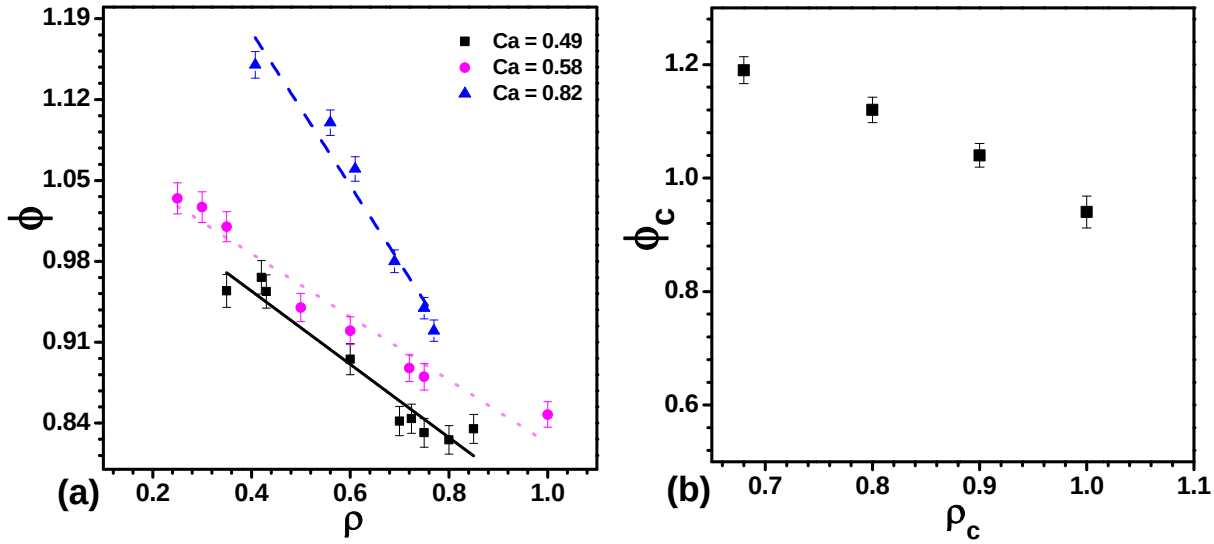

Fig.S4 Variation of mobility of (a) droplets of size ratio ρ for different Ca (b) cells of size ratio ρ_c , flow rate 2.0 µl/min.

Spacing control of objects

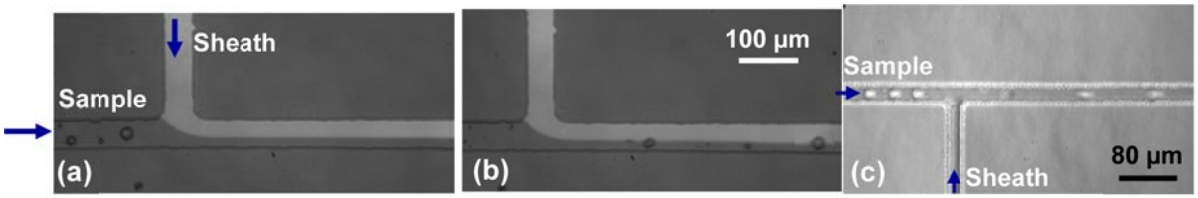

Fig. S5 (a) Droplets of different size ratio at upstream of the T-Junction (region *1*) (b) downstream of the T-junction (region *2*) (Rhodamine dye added to the sheath fluid) (c) Increase in the spacing between a train of droplets (without dye).

The device geometry was determined using the analytical model (reported in section 3.2) and the device performance in terms of separation control and sorting was demonstrated using Ansys-Fluent volume of fluid (VOF) simulations. A detailed description of the numerical model and procedure of VOF simulations are reported in our earlier work[1]. Simulations were performed to observe the time-variation in the spacing between an adjacent pair of equal or unequal size droplets, as depicted in Fig. S6 (a) and (b), respectively. Fig.S6 (a) shows trajectories of a pair of droplets of same size ratio (i.e. relative size ratio ρ_r =1) initially in region *1* and finally in region *2* at a flow rate ratio f_{sc} =1. The spacing

between droplets (i.e. g_2) at various instant of time t is non-dimensionalised with respect to the initial spacing g_1 between the droplets in region *1* and this non-dimensional spacing is denoted by g^*. To calculate time t (presented as horizontal axis in Fig. S6, the instant of time when the leading droplet is about the enter region *2* is taken as t =0.

As observed, in the case of a pair of droplets having equal size ratio ($\rho = 0.75$ and ρ_r =1), before the pair arrives at the spacing control region, the spacing g^* remains fixed and does not vary with time (shown in zone A of Fig.S6(a)). However, at an instant of time when the leading droplet in the pair is about to enter the region *2* (i.e. at $t = 0$), its speed along the channel is reduced which could be because it also attains a transverse velocity component due to the incoming sheath flow. While the leading droplet slows down, the trailing droplet still moves with the same velocity. Thus, there is an instantaneous reduction in the spacing between the pair of droplets g^* at t =0. However, as soon as the leading droplet enters into region *2*, it attains a higher velocity (due to the incoming sheath flow) as compared to the trailing droplet which results in an increase in the spacing g^* between the droplets (shown in zone B of Fig.S6 (a)). The spacing g^* between the droplets keeps on increasing until the trailing droplet also enters the region *2* . As observed, in this case, the increase in the spacing between the droplets g^* takes place over a time period 0-1.875 ms. Once both droplets in a pair (ρ_r =1) get into region *2* , the spacing g^* between them does not change further downstream and remains fixed (shown in zone C of Fig.S6(a)), which is in accordance with the analytical model presented (eqn. S4). However, in a pair of droplets, if a smaller leading droplet is followed by a larger trailing droplet, the spacing between the droplets achieved in region *2* keeps on increasing which is because of mobility contrast between the smaller and larger droplets.

Next, we consider a pair of droplets ($\rho_r = 1.5$) in which the leading droplet is larger ($\rho = 0.75$) and the trailing object is smaller ($\rho = 0.5$) and perform simulations to determine the droplet trajectories at a flow rate ratio f =1. In this case, in region *1,* due to the mobility contrast between the smaller and larger droplets, the spacing between the droplets keeps on decreasing until the leading larger droplets is about to enter the region *2* (zone A of Fig. S6 (b)). The spacing between the droplets is minimum at the instant immediately before the leading droplet enters region *2*. Once the leading larger droplet enters region *2*, due to the incoming sheath flow, the spacing between the droplets keeps on increasing until the trailing smaller droplet enters region *2* (zone B of Fig. S6 (b)). Once the trailing smaller droplet enters the region 2, due to the mobility contrast between the smaller and larger droplets, the spacing between them keeps on decreasing downstream (shown in zone C of Fig. S6 (b)). This is a critical design criterion because the spacing between the droplets should be larger than the length of the sensing channel when the pair of droplets arrives at the sensing channel. The required spacing g^* between a pair of droplets having relative size ratio $\rho_r > 1$ can be predicted using eqn. (S5). For example, a pair of droplets with $\rho_r = 1.5$ and initial spacing of g_1=40 μm will have a final spacing (before entering the sensing channel) less than the length of the sensing channel L_{sen}=100 μm at a flow rate ratio of $f_{sc} = 1.2$. However, if we use a flow rate ratio of $f_{sc} = 3$, the final spacing between the pair of droplets will be higher as compared to the sensing channel length (100 μm).

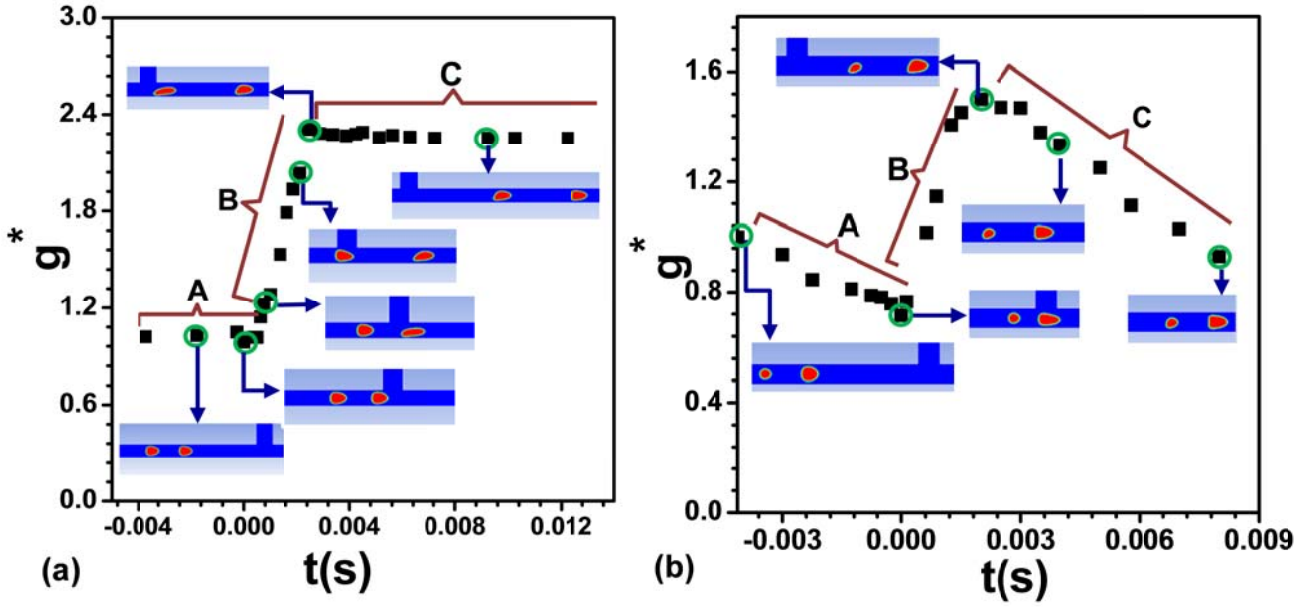

Fig.S6 Trajectory of a pair of droplets during spacing control for flow rate ratio $f = 1$ (relative positions of the droplets shown as inset) (a) droplets of same size ratio $\rho = 0.75$ (b) droplets of different size ratios $\rho = 0.75$ and 0.5 with $\rho_r = 1.5$.

Sorting of droplets and cells

Fig. S7 (a) shows that the device used for sorting of gelatine droplets (main channel size 50×20 µm) is capable of sorting droplets about a threshold size of 17µm whereas Fig. S7 (b) shows that the sorting device used for aqueous glycerol droplets (main channel size 20×20µm) is capable of sorting droplets about a threshold size (diameter) of 6.25µm. Similarly, the device used for sorting of HL60 cells (main channel size 20×20µm) is able to sort cells about a threshold size of 6.0µm, as shown in Fig. S7 (c). In the above devices, mainly the length of the side branch channel can be adjusted to control to side-to-straight branch channel flow rate ratio Q_{si}/Q_{st} , which in turn controls the critical stream width w .

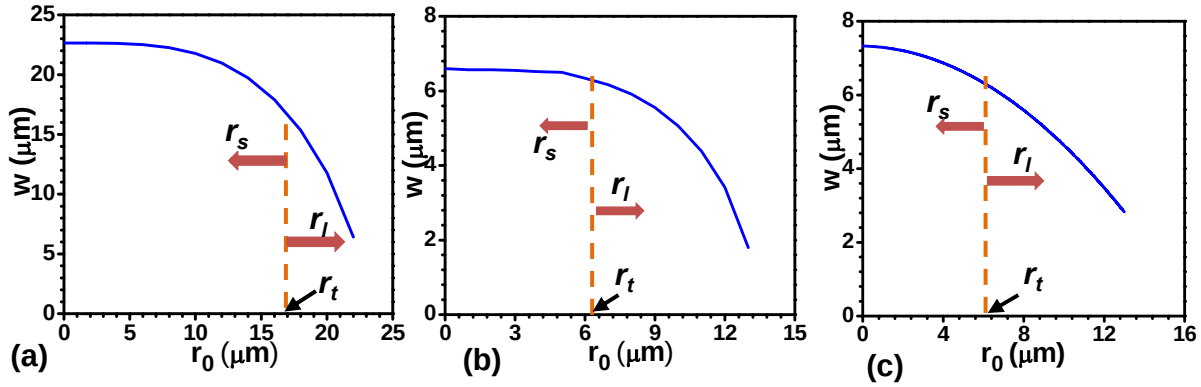

Fig. S7 Variation of the critical width with object size (a) gelatine droplets (b) aqueous glycerol droplets (c) HL60 cells.

The dynamic control of the critical stream width was demonstrated by observing the position of the streamline at the interface between the sheath and sample fluids before the droplet has approached the sensing channel, during the presence of the droplet in the channel and after the droplet leaves the sensing channel, as shown in Fig. S8 (a-c), respectively. The sheath fluid was mixed with a fluorescent dye (Rhodamine dye) and the shifting of the interface was observed (with fluorescence and bright field activated simultaneously) when an object arrives at the sensing channel. DI water was used as the sample fluid. The fluorescence and bright field activation helps in clear visualization of the sheath fluid and the channel (and sample fluid), respectively. As observed, when a droplet of 20 µm size (diameter) enters the sensing channel, the interface between the sheath and sample fluids is shifted down from 25 ±1 µm (shown in Fig. S8 (a)) to 30±1 µm (Fig. S8 (b)). However, as soon as the droplet leaves the sensing channel into the side branch channel (as the radius is less than the dynamic critical stream width), the interface again shifts back to its initial position (Fig. S8(c)).

Next, we demonstrate sorting of aqueous glycerol droplets of 10µm size from that of 15µm size using VOF simulations and experiments. Simulation results showing focusing and separation control and sorting of droplets (10 and 15µm size)

are shown in Fig. S9. As observed, a sheath-to-sample flow rate ratio $f = 1$ is able to focus the two droplets onto the lower side wall and control the spacing between the two droplets (spacing ~188 µm >length of the sensing channel 110µm). The side-to-straight branch channel flow rate ratio is such that the critical stream width is 6.25µm. As observed, the 10µm size droplets are sorted into the side branch channel whereas the 15µm droplets are sorted into the straight branch channel, which also observed from our experiments, as shown in Fig. S10.

In the absence of the bypass channel (i.e. using hydrodynamic filtration only), radius of droplets is comparable to the instantaneous critical width thus it will be difficult to sort as they would have equal chance of entering into either of the branch channels. The critical stream width at the bypass junction is smaller than the radius of the smallest droplets. So even if the size of the smallest droplet is smaller than the width of the bypass channel at the junction, the droplets do not enter the bypass channel due to smaller critical stream width.

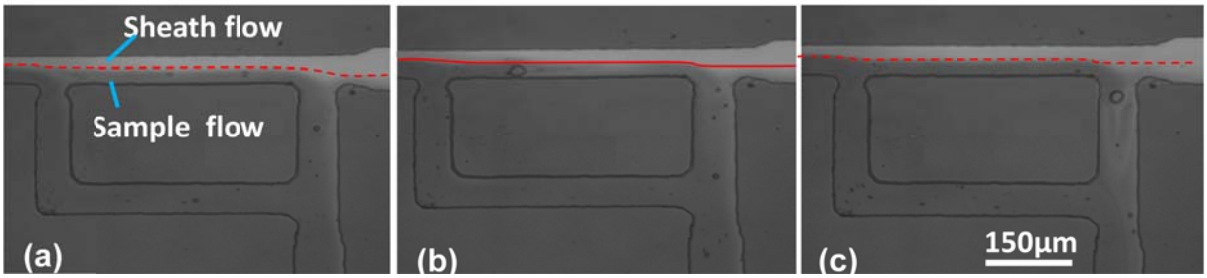

Fig. S8 Experimental images showing shifting of interface in the sensing channel. (a) no droplet present inside the sensing section (b) droplet is present in the sensing section (c) droplet leaving the sensing section.

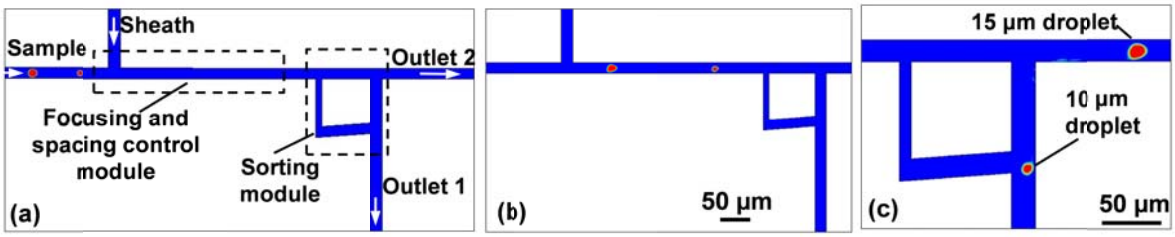

Fig. S9 VOF simulations showing (a) Geometry of the device with different modules (b) Separation control and focusing of droplets to the side wall (c) sorting of 10 µm and 15 µm droplets into side branch and straight branch channels.

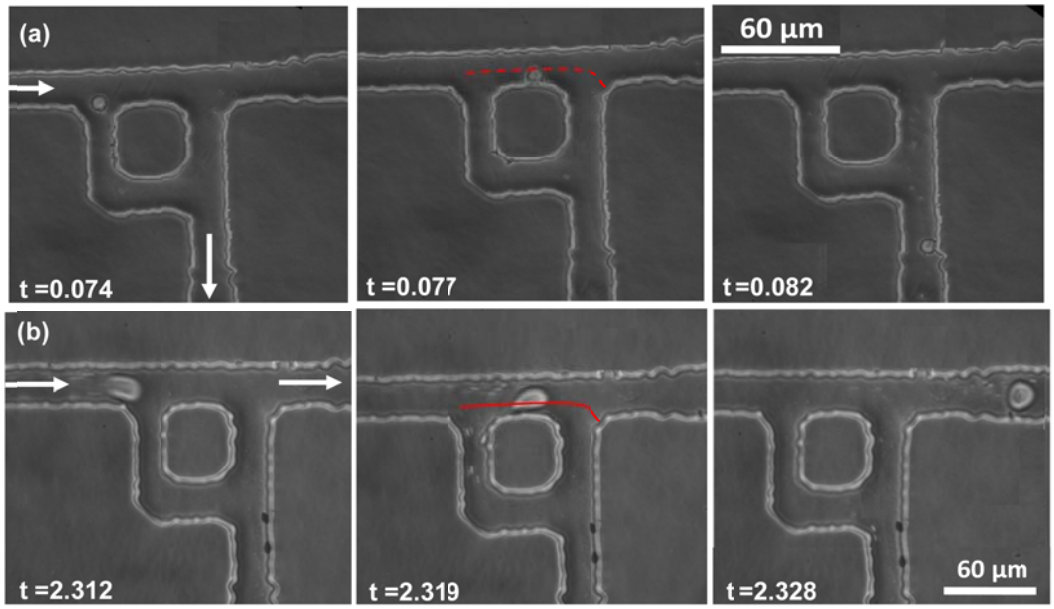

Fig. S10 Experimental images showing (a) trajectory of droplet <10 µm diameter sorted to the side branch channel (b) trajectory of droplet >15 µm diameter sorted into the straight branch channel, position of dividing streamlines shown.

References

1. P. Sajeesh, M. Doble and A. K. Sen, Biomicrofluidics, 2014, **8,** 1–23.
2. H. Bruus, Theoretical microfluidics, Oxford University Press, 2007.